Research Square

Preprints are preliminary reports that have not undergone peer review.
They should not be considered conclusive, used to inform clinical practice,
or referenced by the media as validated information.

Universal monitored dynamics in multimode bosonic systems

Shivam Patel

srp230@scarletmail.rutgers.edu

Rutgers University

Catherine McCarthy

University of Geneva

Ahana Chakraborty

Louisiana State University

Jordan Huang

Rutgers University

Thomas DiNapoli

Rutgers University

Romain Vasseur

University of Geneva

Jedediah Pixley

Rutgers University

Srivatsan Chakram

Rutgers University

Article

Keywords:

Posted Date: July 8th, 2026

DOI: https://doi.org/10.21203/rs.3.rs-10084772/v1

License: This work is licensed under a Creative Commons Attribution 4.0 International License.
Read Full License

Additional Declarations: No competing interests reported.

Universal monitored dynamics in multimode bosonic systems

Shivam Patel,[1,2,*] Catherine McCarthy,[3,†] Ahana Chakraborty,[4,1,2] Jordan Huang,[1] Thomas J. DiNapoli,[1] Romain Vasseur,[3,‡] J. H. Pixley,[1,2,5,§] and Srivatsan Chakram[1,¶]

[1] *Department of Physics and Astronomy, Rutgers University, Piscataway, NJ 08854, USA*
[2] *Center for Materials Theory, Rutgers University, Piscataway, NJ 08854, USA*
[3] *Department of Theoretical Physics, University of Geneva, 24 quai Ernest-Ansermet, 1211 Genève, Switzerland*
[4] *Department of Physics and Astronomy, Louisiana State University, Baton Rouge, Louisiana 70803, USA*
[5] *Center for Computational Quantum Physics, Flatiron Institute, 162 5th Avenue, New York, NY 10010, USA*

(Dated: June 22, 2026)

We propose a route to study monitored many-body dynamics in multimode bosonic systems using circuit quantum electrodynamics. In this experimental setting, we construct several bosonic models comprising brickwork circuits built from beam-splitter gates, local parity measurements, and optional on-site Hubbard interactions, and diagnose their monitored dynamics via ancilla purification and a learnability-based probe. Under parity measurements, generic gate sets exhibit behavior that is largely consistent with a conventional measurement-induced phase transition, while a special class of beam-splitter circuits shows an apparent critical-like high-measurement regime in which purification times scale linearly with system size. We show that for realistic noise, gate, and measurement rates, these signatures are observable with near-term circuit QED hardware.

Rapid experimental progress in quantum devices over the past two decades has produced a range of potential quantum computing platforms—including superconducting circuits, neutral Rydberg-atom arrays, and trapped ions—that can implement coherent unitary dynamics, mid-circuit measurements, and real-time feedback, enabling quantum error correction and heralding the development of future fault-tolerant machines [1–5]. Among these, bosonic circuit quantum electrodynamic (cQED) systems have shown particular promise for hardware-efficient quantum error correction [6–8], leveraging long coherence times [9, 10], large local bosonic Hilbert spaces, fast high-fidelity universal control [11–16], high-fidelity quantum-non-demolition measurements [17], and fast feedback [6].

With the incorporation of mid-circuit measurements and error correction in bosonic cQED platforms, measurement and feedback naturally become part of the dynamics. Monitored many-body dynamics has been extensively studied in qubit-based circuit models, leading to the discovery of the *measurement-induced phase transition* (MIPT) [18–29]: a transition in the entanglement structure of the wavefunction driven by the competition between entangling unitary evolution and local measurements. Signatures of MIPT phenomena have also been probed experimentally, albeit only in qubit platforms to date, in superconducting circuits and trapped ion systems [4, 5, 30, 31].

Monitored free bosons with Gaussian measurements have also begun to attract theoretical attention in recent years [32–34]. However, in random brick-layer bosonic circuits with Gaussian unitaries interspersed with Gaussian measurements, no evidence is found for a MIPT at any finite measurement rate; instead, the system flows to an area-lawentangled phase [35]. This motivates studying monitored bosonic dynamics with *non-Gaussian* ingredients naturally available in cQED, such as parity measurements and interacting gates.

Rapid advancements in the coherence and control of microwave cavity devices in circuit QED now enable access to monitored dynamics in bosonic systems. While most demonstrations of quantum operations have been limited to one or a few modes, recent experiments have also realized multimode bosonic memories that support universal control across many long-lived modes [13, 14, 36, 37]. The large local bosonic Hilbert space presents an opportunity to discover physics that is distinct from the standard qubit case. The bunching of bosons leads to characteristic Hong-Ou-Mandel interference effects [38] and underlies boson sampling [39], where linear, number-conserving beam-splitter dynamics generate nontrivial many-body correlations even in the absence of interactions. The large local Hilbert space also expands the space of operators for measurements, ranging from parity to photon number.

In this work, we advance the understanding of monitored bosonic dynamics on two fronts: we extend numerical analyses to non-Gaussian monitored bosonic evolution, uncovering novel entanglement phases and bosonic MIPTs; and we propose an experimental roadmap for realizing such monitored dynamics on near-term multimode cQED platforms, including a detailed error budget analysis. The circuits studied here are composed of a combination of Gaussian beam-splitter gates, non-Gaussian tunable on-site Hubbard interactions, and local parity measurements. We diagnose the resulting monitored dynamics via the purification of an initially entan-

* co-first author; srp230@scarletmail.rutgers.edu
† co-first author; Catherine.Mccarthy@unige.ch
‡ Romain.Vasseur@unige.ch
§ jed.pixley@physics.rutgers.edu
¶ schakram@physics.rutgers.edu

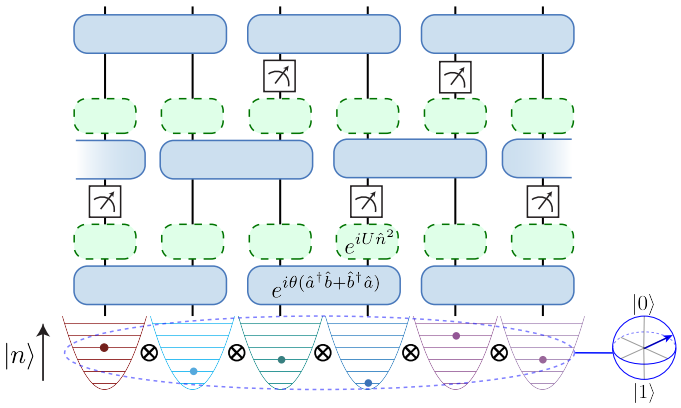


Figure 1. **Multimode bosonic analog of a brick-layer circuit for probing monitored dynamics**. The resonant modes of low-loss superconducting cavities act as harmonic oscillators encoding bosonic degrees of freedom. A reference qubit (dark blue Bloch sphere) is prepared in a globally entangled state with the modes and serves as a probe of the MIPT through its purification dynamics. Each layer applies random beam-splitter gates (light blue), optional on-site Hubbard-like gates (green), and probabilistic mid-circuit measurements (squares with arrows) of parity or photon number.

gled ancillary mode and an alternative learnability probe. For a certain class of beam-splitter unitaries, we uncover behavior unique to the bosonic setting and find numerical evidence for a critical-like monitored phase whose purification time grows linearly with system size. In contrast, for all other types of gates studied here, the dynamics appear consistent with a conventional measurement-induced phase transition between volume- and area-law entanglement (equivalently, between slow and $\mathcal{O}(1)$ purification) as the measurement rate is increased, with a dynamical critical exponent $z \approx 1$. Counterintuitively, we find that increasing the scrambling power of the unitaries *decreases* the purification time of the high-measurement phase, highlighting a rich interplay between unitary dynamics and parity measurements in bosonic systems, where scrambling appears to help measurements reveal information, instead of hiding it [20]. Finally, we assess near-term experimental feasibility on a platform employing the recently-developed cascaded Random Access Quantum Memory (RAQM) architecture [37].

Monitored bosonic circuit-QED toolbox: The class of monitored circuits considered in this work is shown in Fig. 1. They require a register of harmonic modes encoding bosonic degrees of freedom, entangling unitary gates (implemented here between nearest neighbors), and local quantum non-demolition (QND) mid-circuit measurements. The unitary dynamics are chosen to be either (i) purely Gaussian beam-splitter operations or (ii) a combination of beam-splitter dynamics and a (non-Gaussian) local on-site Hubbard interaction. These ingredients can be realized in circuit QED by encoding the bosonic modes in electromagnetic resonances of low-loss superconducting microwave cavities, and by coupling the cavity register to superconducting Josephson circuits that enable high-fidelity control, engineered mode–mode interactions, and QND readout. The cavity resonances can exhibit coherence times ranging from milliseconds [9, 13, 40] to tens of milliseconds in niobium cavities [10, 41–43], and can be engineered to be multimode with tens of addressable resonances [13, 36, 37]. This combination of multimode capacity, long coherence, and high-fidelity control and measurement is crucial for realizing monitored dynamics at depths comparable to the system size.

We implement beam-splitter operations in circuit QED by parametrically activating mode–mode interactions mediated by superconducting Josephson circuits. Such interactions can be engineered using a variety of tunable coupler circuits, which are driven either by a time-dependent voltage drive [16, 44] or a flux drive [37, 45, 46] at the difference frequency of the target cavity modes, realizing programmable beam-splitter gates with errors on the order of $\sim 10^{-3}$. In this way, one can implement nearest-neighbor hopping operations of the form

$$V^{\mathrm{hop}}_{n,n+1}(\theta,\varphi) = \exp\left[i\theta\left(\hat{a}^\dagger_n \hat{a}_{n+1} e^{i\varphi} + \hat{a}^\dagger_{n+1}\hat{a}_n e^{-i\varphi}\right)\right], \tag{1}$$

where $\hat{a}^{(\dagger)}_n$ are the annihilation (creation) operators on site n. The beam-splitter gates are applied for variable durations to implement a swap angle $\theta \in [0, 2\pi]$, while the phase φ is set by the phase of the drive tone. In what follows, it will be important to distinguish between evolutions generated from beam-splitter gates with fixed phases (BSFP) and those with randomized phases (BSRP), since randomizing φ substantially increases the degree of mode mixing (and hence scrambling within a fixed-photon-number sector). This can be seen in the Heisenberg picture: $V^{\mathrm{hop}}_{n,n+1}(\theta,\varphi)$ implements an SU(2) rotation of the operator doublet $(\hat{a}^\dagger_n, \hat{a}^\dagger_{n+1})$, with φ selecting the rotation axis in this two-mode operator space. Fixed-phase gates therefore generate SU(2) rotations about a single axis, while randomizing φ yields rotations about a range of axes, producing more generic mode mixing and state scrambling. We study both BSFP and BSRP circuits. In the presence of parity measurements, BSFP dynamics exhibits an apparent critical-like high-measurement regime, and we therefore focus on this case in the main text; results for BSRP circuits are discussed in the Supplementary Information.

To extend beyond Gaussian dynamics, we exploit the nonlinearity of a superconducting transmon circuit, which yields a dispersive interaction with the coupled cavity modes characterized by a dispersive shift χ. In the dispersive regime, the transmon frequency is shifted by $n\chi$ conditioned on the cavity photon number n. This dispersive interaction enables a broad set of unitary control primitives for the joint transmon–bosonic-mode system [11, 36, 47–49], and provides a unified toolbox for accessing non-Gaussian physics in monitored circuits in two complementary ways: (i) through unitary gates

that implement effective nonlinear interactions, and (ii) through measurement backaction from QND measurements of nonlinear observables (e.g., parity or photon number), which makes individual quantum trajectories non-Gaussian.

We implement nonlinear on-site Hubbard-like interaction gates of the form

$$V_n^{\mathrm{int}}(U) = e^{-iU(\hat{a}_n^\dagger \hat{a}_n)^2}, \tag{2}$$

where U is a dimensionless parameter controlling the strength of the gate. This evolution can, in principle, be realized using a native self-Kerr interaction; however, in circuit-QED systems the self-Kerr is typically small ($\sim$ 10 kHz). We therefore implement these interacting gates via Selective Number-dependent Arbitrary Phase (SNAP) gates [47, 48], where photon-number–selective transmon rotations [50] can be used to implement arbitrary photon-number-dependent geometric phases. In particular, we realize a Hubbard interaction by imprinting a quadratic photon-number–dependent phase. We use a recently developed optimal-control protocol [51] to achieve this operation in a time $3.25/\chi$, where χ is the dispersive interaction strength.

The same dispersive interaction further enables a range of quantum non-demolition (QND) measurements of the cavity modes. In particular, it enables projections onto specific photon-number subspaces [50] using number-resolved transmon π rotations followed by transmon readout. It also enables QND parity measurements [52] via a transmon Ramsey sequence with a dispersive interaction time $T = \pi/\chi$, which maps even and odd cavity parity onto distinct transmon states ($|g\rangle$ and $|e\rangle$). This corresponds to the first bit of the binary representation of the photon number, and higher-order bits (the m^{th} bit) can be obtained by tuning the Ramsey idle time to $T = 1/(2^m\chi)$. A series of adaptive Ramsey measurements with feedforward can then yield a QND photon-number ($\hat{a}^\dagger\hat{a}$) measurement, extracting one bit at a time [53] (see Supplementary Information). Measurements of this type introduce non-Gaussianity into the trajectories; thus, all of the circuit models we study represent non-Gaussian monitored evolutions even when the unitary component is composed only of (Gaussian) beam-splitter gates, in contrast to previous works on monitored free bosons [32–35]. We focus on parity measurements in the main text because they incompletely collapse the local Hilbert space onto Fock basis states, which we will show leads to qualitative differences from the qubit case and novel measurement-induced phenomena.

Monitored Dynamics in Bosonic Circuits: Motivated by the capabilities of the circuit-QED toolbox described above, we now introduce several quantum-circuit models for monitored dynamics in multimode bosonic systems. We consider a brickwork circuit of L bosonic modes (Fig. 1) with a fixed total photon (particle) number Q, so that the Hilbert-space dimension in the fixed-Q sector scales as $N = \binom{Q+L-1}{Q}$. Throughout this work, we fix the filling fraction $Q = L/2$ for chains of L modes so that Q scales extensively with system size and yields a large accessible state space. The dynamics proceeds in discrete layers: each timestep applies a brickwork pattern of two-mode unitary gates, followed by local mid-circuit measurements performed independently on each mode with probability p. The unitary layers are generated from beam-splitter gates with randomized swap angles. The beam-splitter phases are either kept fixed (BSFP) or also randomized (BSRP). In some models, the beam-splitter dynamics is supplemented with an on-site Hubbard interaction (implemented via a SNAP gate). The measurements are chosen to be either QND parity measurements or QND photon-number (density) measurements.

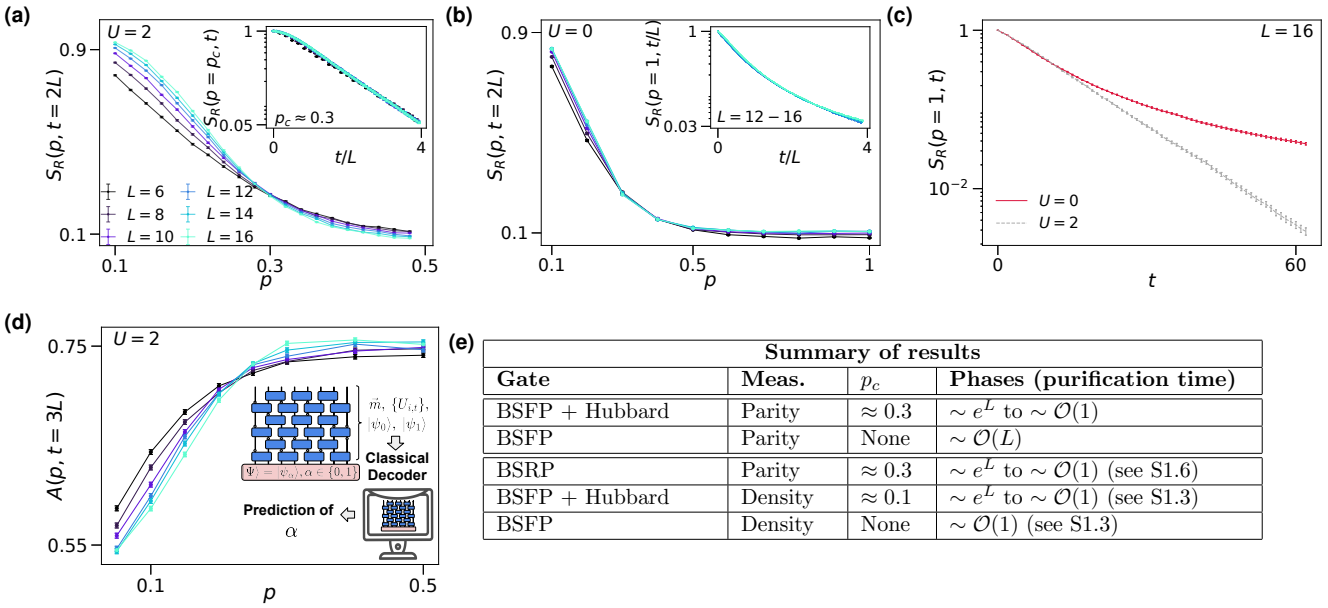
In the main text, we focus on two specific models that highlight both dynamics consistent with previously studied MIPTs in qubit circuits and monitored phenomena specific to bosonic circuits: (i) parity measurements with BSFP gates supplemented by on-site interactions, and (ii) parity measurements with purely BSFP dynamics. In both cases, the unitary evolution conserves total photon number and is generated by repeated application of a two-mode gate of the form

$$\hat{U}_{n,n+1}(\theta, U) = V_{n+1}^{\mathrm{int}}(U)\, V_n^{\mathrm{int}}(U)\, V_{n,n+1}^{\mathrm{hop}}(\theta, 0), \tag{3}$$

where U tunes the strength of the on-site Hubbard interaction, with $U = 0$ corresponding to the non-interacting (pure beam-splitter) limit.

Probing MIPTs through entanglement: The typical method of detecting a MIPT relies on observables that are nonlinear in the system's density matrix ρ and conditioned on the mid-circuit measurement trajectories $\vec{m}$. One such quantity is the entropy of the entanglement of an ancillary reference qubit R with the L modes, which is obtained from preparing the initial state $|\Psi\rangle = \frac{1}{\sqrt{2}}(|\psi_0\rangle\,|0\rangle_R + |\psi_1\rangle\,|1\rangle_R)$, where $|\psi_0\rangle, |\psi_1\rangle$ are orthogonal Haar-random states in the space of states containing $Q = L/2$ bosons. The MIPT is detectable as a transition in the entanglement entropy of R, given by $S_R = -\sum_{\vec{m}} p_{\vec{m}} \mathrm{Tr}[\rho_R \log_2(\rho_R)]$, where ρ_R is the reduced density matrix of R and $p_{\vec{m}}$ is the Born probability of trajectory $\vec{m}$ [28]. A second quantity that is frequently used to diagnose MIPTs is the bipartite entanglement entropy $S = -\mathrm{Tr}[\rho_A \log_2(\rho_A)]$, where A is the first $L/2$ sites of the system– numerical results for the bipartite entanglement entropy are provided in S1.4 [54]. Since the experimental computation of both S_R and S requires post-selecting on individual measurement trajectories, the number of which grows exponentially with system size L, obtaining either quickly becomes experimentally unfeasible for even moderate system sizes.

Learnability as a probe of MIPT: To bypass the need for performing experimental post-selection, we also consider an alternative "learnability" perspective [43, 55–61] which views the MIPT as an information-theoretic transition rather than a transition in the entanglement properties of a quantum state. To probe the learnability transition, we consider a classical decoder tasked with distinguishing between two initially orthogonal random states



(e)

Summary of results			
Gate	**Meas.**	p_c	**Phases (purification time)**
BSFP + Hubbard	Parity	≈ 0.3	$\sim e^L$ to $\sim \mathcal{O}(1)$
BSFP	Parity	None	$\sim \mathcal{O}(L)$
BSRP	Parity	≈ 0.3	$\sim e^L$ to $\sim \mathcal{O}(1)$ (see S1.6)
BSFP + Hubbard	Density	≈ 0.1	$\sim e^L$ to $\sim \mathcal{O}(1)$ (see S1.3)
BSFP	Density	None	$\sim \mathcal{O}(1)$ (see S1.3)

Figure 2. **Monitored dynamics with parity measurements.** Ancilla entanglement entropy S_R for circuits composed of (a) both BSFP and on-site Hubbard gates of strength $U = 2$ and (b) those composed of purely BSFP gates ($U = 0$) for systems of size $L = 4 - 16$, averaged over 10000 independent realizations. For the $U = 2$ case, both the clear crossing of the $S_R(p, t = 2L)$ curves at $p_c \approx 0.3$ and the collapse of $S_R(p_c \approx 0.3, t/L)$ (inset) indicate the presence of a phase transition. In contrast, the $U = 0$ data shows no clear signature of a standard MIPT, with the ancilla not purifying at any value of p at these time scales. In addition, the collapse of $S_R(p, t/L)$ curves for the presented times for $p \gtrsim 0.3$ for the largest numerically-accessible system sizes ($L = 12 - 16$, inset) indicates that at higher measurement rates, the system is in a phase with a purification time that scales with system size. (c) Comparison of $S_R(p = 1, t)$ between the $U = 2$ and $U = 0$ cases. Turning on the on-site Hubbard gates takes the system from a phase in which the purification time scales with system size ($U = 0$) to a phase with an $\mathcal{O}(1)$ purification time ($U = 2$). **Learnability** (d) Simulated decoder accuracy $A(p)$ for monitored dynamics with BSFP and on-site Hubbard gates ($U = 2$). The accuracy $A(p)$ shows a similar transition to the ancilla entanglement entropy S_R in (a) and may be used as an alternative post-selection free order parameter. Inset: protocol for detecting the learnability transition. A monitored circuit is run in the lab using an initial state of either $|\psi_0\rangle$ or $|\psi_1\rangle$, where $\langle\psi_0|\psi_1\rangle = 0$. A classical decoder then outputs a prediction of the initial state given the measurement record $\vec{m}$, the gates, and knowledge of $|\psi_0\rangle, |\psi_1\rangle$. **Summary table** (e) Summary of all numerical results. For non-BSFP gates with any measurement type, the data is consistent with a standard MIPT. In contrast, the purely BSFP gates are consistent with either a critical phase at high p (parity measurements) or a purified phase at any p (density measurements); "None" refers to the lack of an MIPT with $z = 1$.

$|\psi_0\rangle, |\psi_1\rangle$ given a measurement record $\vec{m}$ of a monitored trajectory generated with the set of unitaries $\{U_{i,t}\}$, as illustrated in the inset of Fig. 2(d). The transition appears in the accuracy of this decoder $A(p) = \frac{1}{N}\sum_n a(n,p)$, where $a(n,p) \in \{0,1\}$ is a binary variable that tracks the success of the decoder for the n^{th} record generated with measurement rate p– see S1.2 for implementation details. The advantage of the learnability perspective is that the exponential difficulty is shifted from an experimental task (post-selection) to a numerical task (the implementation of the decoder), which may permit moderate increases in experimentally-accessible system sizes.

Interacting circuits with BSFP and on-site Hubbard gates: We first consider a brick layer monitored circuit evolving with both BSFP and on-site Hubbard gates ($U = 2$) with parity measurements. The (post-selected) ancilla entanglement entropy is shown in Fig. 2(a) for parity measurements for varying system sizes $L = 8 - 16$. The S_R curves are consistent with a transition with $z = 1$ at $p_c \approx 0.3$, as demonstrated by the crossing in $S_R(p, t \sim L^z)$ and the collapse of the $S_R(p = p_c, t/L^z)$ curves for (Fig. 2a). This behavior is similar to that of a standard MIPT, in which there is a transition from an exponentially-long to $\mathcal{O}(1)$ purification time in the ancilla R. The results of the learnability probe are consistent with the S_R data, as shown in S1.2.

Qualitatively, the S_R and learnability results appear to be representative of generic bosonic monitored dynamics. For instance, choosing different values of $U > 0$ or choosing to perform full number measurements may alter the location of p_c but does not appear to affect the existence of a transition or the different phases. The same appears to be true for circuits generated from purely beamsplitter with random φ (BSRP) gates, indicating that non-Gaussian gates are not a requirement for observing a bosonic MIPT and the non-Gaussianity from measurements is sufficient– see Table in Fig. 2(e).

Purely BSFP circuits: In contrast to the $U = 2$ case,

the monitored dynamics generated from only BSFP gates ($U = 0$) is strikingly different. Fig. 2(b) shows the data for the entanglement entropy of the ancilla qubit for evolution with BSFP gates together with parity measurement which is *inconsistent* with a standard MIPT with $z = 1$. The ancilla never purifies at any p on timescales $t \sim L$, as most strikingly demonstrated at $p = 1$. Furthermore, we find that $S_R(p, t/L)$ collapses on time scales $t \sim L$ [Fig. 2(b) inset] for an entire range of large-p values for the largest numerically-accessible system sizes ($L = 12 - 16$). This collapse is consistent with a novel phase in which the ancilla purifies on $\mathcal{O}(L)$ timescales– given that this scaling is normally seen only at a single p_c, we refer to this phase as a *critical phase*. The contrast between the $U = 0$ and $U = 2$ curves for $S_R(p = 1, t)$ (Fig. 2(c)) demonstrates that the BSFP gate is a special case and that choosing a more generic gate restores the conventional high-measurement phase with ancilla purification on $\mathcal{O}(1)$ timescales. We note that this critical phase also requires the limited projective nature of the parity measurements– if we instead consider density measurements, we find the ancilla always purifies at a time scale of $\mathcal{O}(1)$ (see S1.3 [54]).

While we find numerical evidence for a critical phase at high measurement rates from the $U = 0$ data, we are unable to identify any clear signature of a transition from some other (possibly mixed) phase to this critical phase. Two possibilities are that the system is that the critical phase endures across all values of p or that there is a transition with $z > 1$ (see S1.5 for preliminary discussion). As demonstrated by recent work on free-fermions, inferring a critical phase from numerical data from finite system sizes is challenging [62]– it is possible that the apparent critical phase is an artifact of the small numerically-accessible system sizes. Future analytical work is necessary to distinguish among these possibilities.

Scrambling with parity measurements: MIPTs are often understood as a competition between scrambling unitary dynamics, which dominates in the mixed phase, and the disentangling effect of measurements, which dominates in the purified phase. With this intuition, choosing more scrambling gates would be expected to favor the mixed phase. Our data displays the opposite trend: either by adding on-site Hubbard gates to a BSFP evolution or by using only BSRP gates, both of which are *increase* scrambling compared to the purely BSFP case, the purification time of the high-measurement phase *decreases* from $\mathcal{O}(L)$ to $\mathcal{O}(1)$. This effect arises from the fact that parity measurements project onto a subspace of the local Hilbert space, rather than onto a single Fock basis state. Therefore, scrambling in between repeated parity measurements creates more opportunities to collapse the state and thus reduce its entanglement entropy– see S2 for further discussion [54].

Bipartite entanglement entropy: We provide results for the bipartite entanglement entropy S for both the $U = 0$ and $U = 2$ cases in S1.4. Intriguingly, for both cases, S does not show any clear signature of a transition and is possibly consistent with critical $\sim \log L$ scaling at high measurement rates. Although the coincidence of the apparent $\log L$ phase for S and the critical phase for S_R is consistent for the $U = 0$ case, the $U = 2$ case is more puzzling. While inferring $\sim \log L$ scaling from numerics limited to small system sizes is challenging [62], the data raises the intriguing possibility that there is a decoupling between the ancilla and bipartite entanglement transitions, a scenario which is left for future research.

Realizing Bosonic MIPT with Multimode Circuit QED: We consider two representative experimental platforms for realizing the theoretical bosonic circuit models. The first platform, shown in Fig. 3(a), consists of a 1D array of coaxial $\lambda/4$ cavities [9] coupled by tunable couplers [16, 37, 45] that enable nearest-neighbor beam-splitter operations [63, 64]. Each cavity is also interfaced with its own transmon ancilla, coupled to a readout resonator, which can implement on-site interactions and mid-circuit measurements. This architecture supports parallel gate execution on distinct modes, but it is expensive in control hardware, requiring an ancilla qubit and a coupler element for each mode.

The second platform, shown in Fig. 3(b), is a cascaded random access quantum memory (RAQM) architecture [37], in which a high-coherence multimode storage cavity is coupled via a tunable coupler to a separate buffer cavity that serves as a cache memory and is, in turn, coupled to a transmon. The tunable coupler swaps states between storage modes and buffer modes. In the buffer cavity, the transmon enables universal cavity control (e.g., SNAP gates) and QND measurements of the mode, such as parity measurements, as shown in Fig. 3(d,e). The tunable coupler also enables entangling beam-splitter operations between storage modes, as shown in Fig. 3(c). By isolating the nonlinearity to the buffer/measurement cavity, this architecture suppresses spurious Kerr and cross-Kerr interactions among the storage modes, mitigating error propagation and reducing crosstalk during gate operations. Furthermore, we expect any residual interaction-induced phases to not qualitatively affect the monitored dynamics.

Preparation of the initial state: The numerical analysis of monitored bosonic circuits discussed earlier and shown in Fig. 2 begins from a Haar-random state in the fixed-charge sector with $Q = L/2$ photons. We find that quantitatively similar results can also be obtained by starting from a "checkerboard" state that is globally entangled with a reference qubit and then scrambling with $\mathcal{O}(L)$ layers of beam-splitter and on-site Hubbard gates, as justified numerically in S1.1 and S.6 [54]. The checkerboard state $|\Psi\rangle = \frac{1}{\sqrt{2}} \left(|101010\cdots\rangle |1\rangle_R + |010101\cdots\rangle |0\rangle_R \right)$ entangles two orthogonal alternating-occupancy configurations of the storage-cavity modes with the $|0\rangle$ and $|1\rangle$ states of a reference qubit. In the RAQM architecture, this reference qubit is prepared in the transmon and then swapped into an additional ancillary storage mode (reference mode).

The checkerboard state can be prepared in the RAQM

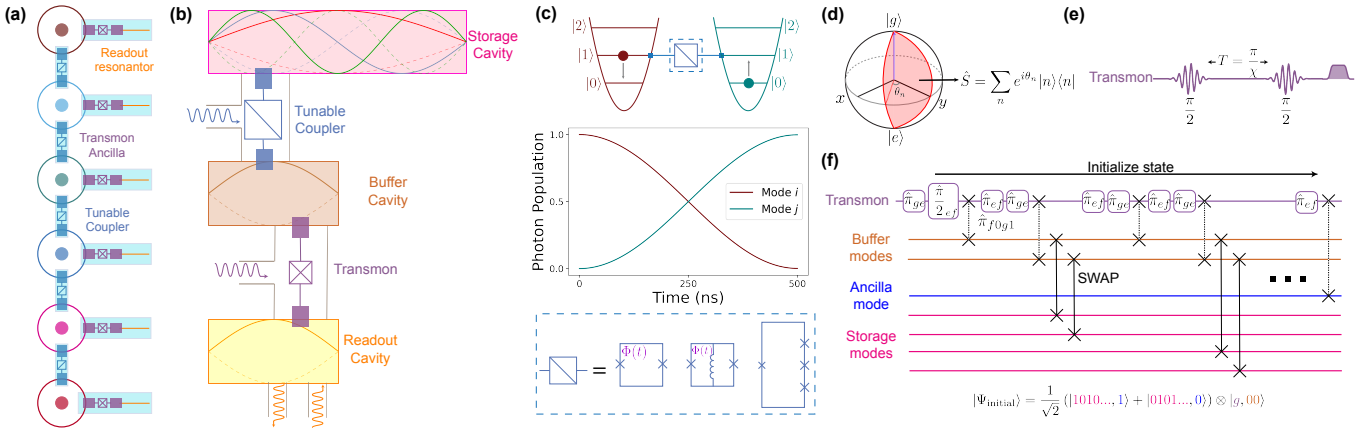


Figure 3. **Linear cavity array architecture** (a) Schematic of a 1D $\lambda/4$ cavity array coupled via tuneable couplers. Each cavity is also interfaced with a chip hosting a transmon and readout cavity. **Cascaded RAQM architecture** (b) Multimode cQED setup of a cascaded random access quantum memory (RAQM) architecture. A superconducting storage cavity coupled to a buffer cavity via a tunable coupler; the buffer cavity is interfaced with a readout resonator through a transmon. **Beam-splitter gate**(c) Cavity modes modeled as harmonic oscillators are coupled via a tunable coupler (ex. SQUID, LINC, or SNAIL) (dashed box). Using a SNAIL we realize a 250 ns beam-splitter gate creating an entangled $\frac{1}{\sqrt{2}}(|10\rangle + |01\rangle)$ state between the modes, and 500 ns SWAP gate. **SNAP gate** (d) SNAP operations, used to realize on-site Hubbard gates, apply geometric photon-number-dependent phases by driving the transmon qubit in a closed trajectory (shaded red) around the Bloch sphere in each photon number subspace. **Parity measurement** (e) Ramsey-based nondemolition photon-number parity readout using dispersive coupling, where two $\pi/2$-pulses are separated by some idle time $T = \pi/\chi$. **State preparation** (f) Pulse sequence for initializing a checkerboard-like state in the storage cavity entangled with a passive reference mode, using π_{ge}/π_{ef} pulses, $f0g1$ sidebands, and coupler-mediated photon shuttling.

architecture using standard protocols used in circuit QED. We harness the quartic nonlinearity of the transmon to implement a four-wave mixing parametric process that converts two excitations in the transmon (the $|f\rangle$ level) into a single photon in the dispersively coupled buffer cavity mode via an $|f0\rangle - |g1\rangle$ sideband transition [12, 36, 65]. This is implemented by applying an external charge drive to the transmon at the difference frequency between the $|f0\rangle$ and $|g1\rangle$ states. By combining these sideband operations with transmon rotations on the $|g\rangle - |e\rangle$ and $|e\rangle - |f\rangle$ transitions, and temporary shelving of the population in the $|e\rangle$ manifold [36], we generate an entangled state between the transmon and the $\{|01\rangle, |10\rangle\}$ state of the pair of buffer modes. The photons in the buffer modes are then swapped into a pair of modes of the storage cavity via the tunable coupler, and this procedure is repeated to populate the storage cavity up to half-filling while maintaining entanglement with the transmon. Finally we swap the transmon state into the ancillary reference mode of storage cavity. A schematic of the full state-preparation sequence is shown in Fig. 3(f) and detailed further in S6. The execution time of the state-preparation protocol scales as $\sim L^2$ and is 4.5 μs for $L = 4$. After the checkerboard state is prepared, we apply $S = 2L$ scrambling layers of nearest-neighbor beam-splitter gates followed by on-site Hubbard gates (implemented via SNAP gates) which provides an initial state that is sufficiently scrambled for the monitored dynamics.

Implementation of monitored bosonic dynamics: We now subject the scrambled input state to our monitored bosonic circuit model, as shown in Fig. 1. We apply $M = 2L$ monitored layers, where each layer consists of a set of BSFP gates and on-site Hubbard gates (for the $U = 2$ case), followed by mid-circuit parity measurements performed independently on each mode with probability p. Measurement outcomes are obtained by reading out the transmon through its readout cavity and are recorded to define the measurement trajectory for each circuit run. All operations are performed sequentially in the RAQM architecture. For SNAP operations and parity measurements, which are transmon-mediated, we swap the target modes from the storage cavity to the buffer cavity, execute the operation, and then swap the modes back into storage. The transmon is reset to its ground state before the next operation. The total execution time of the monitored circuit scales as $\sim L^2$ and, for $L = 4$ and $p = 1$, is $\sim$ 100 μs for the BSFP case and $\sim$ 150 μs for the case with on-site Hubbard gates. Implementations of the gate operations and details of the protocol sequence on the RAQM architecture are described in S8.5.

Measuring the entanglement entropy of the reference mode: After completing the full sequence of gates and measurements, we extract the entanglement entropy of the reference mode, conditioned on the mid-circuit measurement record. Because the reference mode is restricted to the $|0\rangle, |1\rangle$ subspace, its state can be swapped through the buffer cavity into the transmon and fully characterized using standard qubit tomography. Extensions to alternative encodings (e.g., using $|0\rangle$ and $|2\rangle$) en-

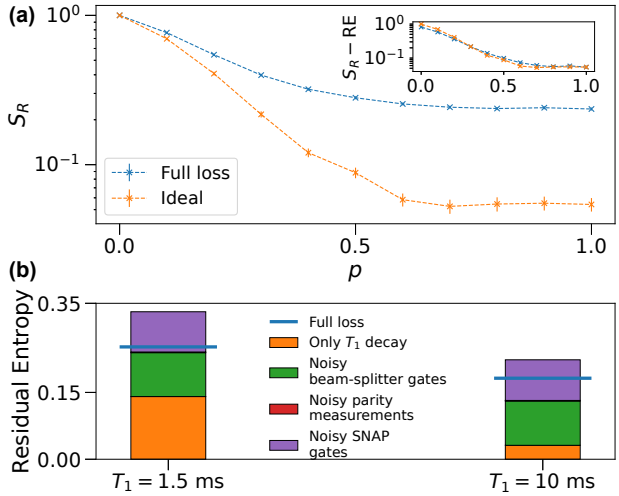


Figure 4. **Effects of noise in monitored bosonic circuits.**(a) Averaged entropy curves for a model containing both BSFP and on-site Hubbard gates with 8 scrambling and 8 monitored layers. Results are shown for ideal gates (orange) and for circuits with all noise sources active (blue). Inset: the same curves after subtracting the residual entropy (RE) from the full loss curve. (b) Breakdown of residual entropies generated at $p = 1$ (for a worst case estimate), obtained from simulations in which a single noise source is active at a time.

able error-detection schemes that can improve the fidelity of the density-matrix reconstruction, at the expense of additional shots [66]. The reconstructed density matrix is then used to compute the entanglement entropy.

For a given measurement rate p, system size L, and random realization of beam-splitter angles, the total number of mid-circuit measurements scales as $m \sim L^2 p$, yielding 2^m possible measurement trajectories. Assuming state-of-the-art single-shot readout fidelity ($\sim 99\%$), we acquire ~ 500 shots per trajectory to reconstruct the ancilla reduced density matrix; this requires executing the monitored circuit 500×2^m times for each of 200 independent realizations of the random unitaries, thereby sampling over both circuit instances and their associated measurement trajectories. Tomography results are binned by the observed measurement record, producing a reconstructed density matrix for each trajectory, from which the entanglement entropy is computed. After each run, the system is reset; tomography and reset are estimated to require approximately 2 μs and 50 μs, respectively [36, 37]. The total runtime of a single monitored-circuit execution, from state preparation to system reset, is approximately 160 μs for the BSFP case and 210 μs for the case with on-site Hubbard gates (for $p = 1$ and $L = 4$). For these parameters, this corresponds to a total acquisition time on the order of a few hundred hours.

Feasibility of the experiment: We assess the feasibility of observing a MIPT in a realistic circuit-QED architecture in the presence of coherent and incoherent gate errors by performing end-to-end simulations of the proposed monitored bosonic circuits. We model noise at the level of elementary operations using Lindblad master-equation simulations that capture the dominant incoherent processes: cavity decay and thermal excitation, transmon relaxation and thermal excitation, and transmon dephasing. Each operation is simulated on the minimal local subsystem on which it acts: beam-splitter gates are simulated on a pair of cavity modes, while parity measurements and on-site Hubbard gates are simulated on a single cavity mode dispersively coupled to a two-level transmon. From these simulations, we extract quantum channels for each noisy operation, embed them into a larger composite Hilbert space, and apply them sequentially in a full circuit-level simulation. These circuit simulations do not include additional dephasing from many-body interactions, which we assume can be engineered to be sufficiently small [37]. The circuit and cavity parameters used in these simulations, which set the relevant gate time scales, are summarized in Tables I and II of S8.

We assume readily achievable thermal populations ($n_{\mathrm{th}} \sim 0.5\%$), coherence times for the transmon ($T_1, T_2 = 200, 50$ μs) and tunable coupler ($T_1, T_2 = 50, 4.2$ μs), and two cavity-coherence regimes, with mode lifetimes of 1.5 ms achievable in aluminum cavities [9, 13] and 10 ms in niobium cavities [10, 43]. At these coherence levels, beam-splitter gate fidelities exceed 0.999 and can be achieved in 250 ns, as has been demonstrated experimentally [16, 45, 46]. We simulate circuits with $L = 4$ cavity modes, $S = 8$ scrambling layers, and $M = 8$ monitored layers with random parity measurements. We model the modes as harmonic oscillators with a truncated local Hilbert-space dimension of $L/2 + 1 = 3$ to include all possible local configurations (0, 1, or 2 photons). The total dimension of the doubled Hilbert space for four modes, a reference qubit, and a transmon qubit is $\approx 10^5$, highlighting the substantial computational complexity of simulating the full open-system dynamics.

Using this noise model, we simulate beam-splitter circuits with and without on-site Hubbard gates during the monitored portion, and we identify the dominant error sources by selectively enabling individual noise channels. We verify that, before the noise channels are turned on, the numerical results for circuits with $L = 4$ modes match the ideal simulation data generated in the same way as the S_R curves in Fig. 2. In all cases, noise produces a finite residual entropy that lifts the saturation value of the ideal entropy curves at large measurement rates. For monitored circuits containing on-site Hubbard gates (implemented via SNAP), we find that cavity T_1 decay and imperfections in the BSFP and on-site Hubbard gates dominate the residual entropy. At lower cavity lifetimes ($T_1 = 1.5$ ms), idle decay of spectator modes and the reference mode during sequential gate applications is the leading error source; increasing the lifetime to 10 ms suppresses this contribution, leaving BSFP and on-site Hubbard gate errors as the dominant source of residual entropy, as shown in Fig. 4(b). Unlike the RAQM architecture, the linear cavity array discussed above supports parallel gate execution and can therefore mitigate this

idling-T_1 contribution by reducing the time modes spend inactive between operations. Beam-splitter circuits without on-site Hubbard gates exhibit the same qualitative trends but with smaller residual entropies due to shorter experimental wall times, since they do not require SNAP gates. Additional details on the error budgets for all monitored circuits considered are provided in S8.5. We note that the qualitative behavior of the ideal dynamics can be approximately recovered by subtracting the noise-induced residual, as shown in the inset of Fig. 4(a), similar to what has been done in qubit realizations of MIPTs [30].

Discussion: We have theoretically investigated monitored dynamics in bosonic systems and outlined feasible experimental protocols for probing MIPTs on current 3D circuit QED platforms. For small system sizes, Lindbladian simulations incorporating decay, thermal excitation, and dephasing errors on both the cavity modes and the coupler and ancilla circuits indicate that the experiment is within reach of existing hardware [37]. Noise induces a excess residual entanglement entropy of the reference mode at high measurement rates, which can be subtracted off [30], allowing for the recovery of the underlying ideal behavior. Although our simulations do not include errors arising from state preparation or ancilla tomography, these errors are not expected to qualitatively alter the transition, but rather increase statistical overhead and experimental runtime. Ancilla tomography errors may be mitigated through error-detectable encoding schemes [67].

By embedding existing schemes for high-fidelity gate operations driven by superconducting circuits [16, 45, 51] into a multimode architecture with tens of high-coherence bosonic modes, this proposal enables access to a regime of monitored dynamics that is inaccessible on qubit-based platforms. This novelty arises from the bosonic statistics of the cavity modes, which permit bosons to bunch in individual modes and allow for the projective strength of measurements to be tuned from parity to full number resolution. As demonstrated in our results, this flexibility alters the nature of the bosonic MIPT. In the case of parity measurements, our numerical results indicate that there are standard purification transitions for most types of unitary gates, while dynamics generated from only BSFP gates exhibit a new phase at high measurement rates in which the ancilla purifies at timescales that scale as the system size. We identify the effect that choosing more scrambling gates enhances the purification process, an effect that has no analogue in qubit systems. Furthermore, for generic, non-BSFP gates, we numerically observe an apparent co-existence between a phase in which the ancilla purifies on $\mathcal{O}(1)$ timescales and a phase in which the bipartite entanglement seems to scale logarithmically with system size, which raises a host of interesting questions.

Other interesting questions include how the filling fraction affects the nature (or existence) of the transition and whether ancilla purification and bipartite entanglement diagnose distinct phases for generic gates at high measurement rates. As demonstrated in studies of both interacting and free fermions, numerically identifying transitions from finite-size data can be subtle [62, 68–72], underscoring the need for complementary analytical understanding of monitored bosonic circuits. Elucidating the mechanisms underlying bosonic MIPTs and their broader implications is an important direction for future research. For example, the existence of a MIPT under beam-splitter dynamics with random phases (see S1.6)—closely related to boson-sampling dynamics and number-conserving gate operations in arrays of dual-rail qubits—motivates exploring possible connections between the observed transition and (i) the classical simulability of monitored beam-splitter dynamics, e.g. via the computational cost of sampling from the conditional output distribution, and (ii) fault-tolerance thresholds for dual-rail erasure codes.

Acknowledgments: C.M. thanks Kabir Khanna for helpful conversations and acknowledges support from NSF GRFP-1938059. S.P acknowledges support from NSF GRFP-2233066. J.H., T.D., and S.C were supported by the Army Research Office under Grant Number W911NF-23-1-0096 and W911NF-23-1-0251. This work was partially supported by the U.S. Department of Energy, Office of Science, National Quantum Information Science Research Centers, Superconducting Quantum Materials and Systems Center (SQMS), under Contract No. 89243024CSC000002. This work was partially supported by the Army Research Office Grant No. W911NF-23-1-0144 (J.H.P.), the US-ONR grant No. N00014-23-1-2357 (S.P. and J.H.P.).

Author Contribution Statement: S.P. and C.M. contributed equally to this work. J.H.P. and S.C. conceived the project. S.P. and S.C. contributed primarily to the experimental protocol design, modeling, and feasibility analysis of the proposed circuit-QED implementation, with contributions from J.H. and T.J.D. C.M., A.C., R.V., and J.H.P. contributed primarily to the theoretical formulation, numerical simulations, and analysis of the numerical results. R.V., J.H.P., and S.C. supervised the project. All authors contributed to broader discussions, interpretation of the results, and manuscript preparation.

[1] J. I. Cirac and P. Zoller, "Quantum computations with cold trapped ions," Phys. Rev. Lett. **74**, 4091–4094 (1995).

[2] M. Saffman, T. G. Walker, and K. Mlmer, "Quantum information with rydberg atoms," Reviews of Modern Physics **82**, 23132363 (2010).

[3] Frank Arute, Kunal Arya, Ryan Babbush, Dave Bacon, Joseph C Bardin, Rami Barends, Rupak Biswas, Sergio

Boixo, Fernando GSL Brandao, David A Buell, *et al.*, "Quantum supremacy using a programmable superconducting processor," Nature **574**, 505–510 (2019).

[4] Crystal Noel, Pradeep Niroula, Daiwei Zhu, Andrew Risinger, Laird Egan, Debopriyo Biswas, Marko Cetina, Alexey V Gorshkov, Michael J Gullans, David A Huse, *et al.*, "Measurement-induced quantum phases realized in a trapped-ion quantum computer," Nature Physics **18**, 760–764 (2022).

[5] Google Quantum AI and Collaborators, "Measurement-induced entanglement and teleportation on a noisy quantum processor," Nature **622**, 481–486 (2023).

[6] Nissim Ofek, Andrei Petrenko, Reinier Heeres, Philip Reinhold, Zaki Leghtas, Brian Vlastakis, Yehan Liu, Luigi Frunzio, SM Girvin, L Jiang, *et al.*, "Extending the lifetime of a quantum bit with error correction in superconducting circuits," Nature **536**, 441–445 (2016).

[7] Ling Hu, Yuwei Ma, Weizhou Cai, Xianghao Mu, Yuan Xu, Weiting Wang, Yukai Wu, Haiyan Wang, YP Song, C-L Zou, *et al.*, "Quantum error correction and universal gate set operation on a binomial bosonic logical qubit," Nature Physics **15**, 503–508 (2019).

[8] Philippe Campagne-Ibarcq, Alec Eickbusch, Steven Touzard, Evan Zalys-Geller, Nicholas E Frattini, Volodymyr V Sivak, Philip Reinhold, Shruti Puri, Shyam Shankar, Robert J Schoelkopf, *et al.*, "Quantum error correction of a qubit encoded in grid states of an oscillator," Nature **584**, 368–372 (2020).

[9] Matthew Reagor, Wolfgang Pfaff, Christopher Axline, Reinier W. Heeres, Nissim Ofek, Katrina Sliwa, Eric Holland, Chen Wang, Jacob Blumoff, Kevin Chou, Michael J. Hatridge, Luigi Frunzio, Michel H. Devoret, Liang Jiang, and Robert J. Schoelkopf, "Quantum memory with millisecond coherence in circuit QED," **94**, 014506, publisher: American Physical Society.

[10] Ofir Milul, Barkay Guttel, Uri Goldblatt, Sergey Hazanov, Lalit M. Joshi, Daniel Chausovsky, Nitzan Kahn, Engin iftyrek, Fabien Lafont, and Serge Rosenblum, "Superconducting cavity qubit with tens of milliseconds single-photon coherence time," **4**, 030336, publisher: American Physical Society.

[11] Reinier W Heeres, Philip Reinhold, Nissim Ofek, Luigi Frunzio, Liang Jiang, Michel H Devoret, and Robert J Schoelkopf, "Implementing a universal gate set on a logical qubit encoded in an oscillator," Nature Communications **8**, 94 (2017).

[12] Serge Rosenblum, Yvonne Y Gao, Philip Reinhold, Chen Wang, Christopher J Axline, Luigi Frunzio, Steven M Girvin, Liang Jiang, Mazyar Mirrahimi, Michel H Devoret, *et al.*, "A cnot gate between multiphoton qubits encoded in two cavities," Nature communications **9**, 652 (2018).

[13] Srivatsan Chakram, Andrew E. Oriani, Ravi K. Naik, Akash V. Dixit, Kevin He, Ankur Agrawal, Hyeokshin Kwon, and David I. Schuster, "Seamless high- q microwave cavities for multimode circuit quantum electrodynamics," **127**, 107701 ().

[14] Srivatsan Chakram, Kevin He, Akash V. Dixit, Andrew E. Oriani, Ravi K. Naik, Nelson Leung, Hyeokshin Kwon, Wen-Long Ma, Liang Jiang, and David I. Schuster, "Multimode photon blockade," **18**, 879–884 (), publisher: Nature Publishing Group.

[15] Yvonne Y Gao, Brian J Lester, Kevin S Chou, Luigi Frunzio, Michel H Devoret, Liang Jiang, SM Girvin, and Robert J Schoelkopf, "Entanglement of bosonic modes through an engineered exchange interaction," Nature **566**, 509 (2019).

[16] Benjamin J. Chapman, Stijn J. De Graaf, Sophia H. Xue, Yaxing Zhang, James Teoh, Jacob C. Curtis, Takahiro Tsunoda, Alec Eickbusch, Alexander P. Read, Akshay Koottandavida, Shantanu O. Mundhada, Luigi Frunzio, M.H. Devoret, S.M. Girvin, and R.J. Schoelkopf, "High-on-off-ratio beam-splitter interaction for gates on bosonically encoded qubits," **4**, 020355.

[17] Thomas Connolly, Pavel D Kurilovich, Vladislav D Kurilovich, Charlotte GL Bøttcher, Sumeru Hazra, Wei Dai, Andy Z Ding, Vidul R Joshi, Heekun Nho, Spencer Diamond, *et al.*, "Full characterization of measurement-induced transitions of a superconducting qubit," arXiv preprint arXiv:2506.05306 (2025).

[18] Yaodong Li, Xiao Chen, and Matthew P. A. Fisher, "Quantum zeno effect and the many-body entanglement transition," Physical Review B **98** (2018), 10.1103/physrevb.98.205136.

[19] Yaodong Li, Xiao Chen, and Matthew PA Fisher, "Measurement-driven entanglement transition in hybrid quantum circuits," Physical Review B **100**, 134306 (2019).

[20] Brian Skinner, Jonathan Ruhman, and Adam Nahum, "Measurement-induced phase transitions in the dynamics of entanglement," Physical Review X **9** (2019), 10.1103/physrevx.9.031009.

[21] Andrew C. Potter and Romain Vasseur, "Entanglement dynamics in hybrid quantum circuits," in *Entanglement in Spin Chains* (Springer International Publishing, 2022) p. 211249.

[22] Matthew PA Fisher, Vedika Khemani, Adam Nahum, and Sagar Vijay, "Random quantum circuits," Annual Review of Condensed Matter Physics **14**, 335–379 (2023).

[23] Amos Chan, Rahul M. Nandkishore, Michael Pretko, and Graeme Smith, "Unitary-projective entanglement dynamics," Physical Review B **99** (2019), 10.1103/physrevb.99.224307.

[24] Michael J. Gullans and David A. Huse, "Dynamical purification phase transition induced by quantum measurements," Physical Review X **10** (2020), 10.1103/physrevx.10.041020.

[25] Yimu Bao, Soonwon Choi, and Ehud Altman, "Theory of the phase transition in random unitary circuits with measurements," Physical Review B **101** (2020), 10.1103/physrevb.101.104301.

[26] Chao-Ming Jian, Yi-Zhuang You, Romain Vasseur, and Andreas W. W. Ludwig, "Measurement-induced criticality in random quantum circuits," Physical Review B **101** (2020), 10.1103/physrevb.101.104302.

[27] Aidan Zabalo, Michael J Gullans, Justin H Wilson, Sarang Gopalakrishnan, David A Huse, and JH Pixley, "Critical properties of the measurement-induced transition in random quantum circuits," Physical Review B **101**, 060301 (2020).

[28] Michael J. Gullans and David A. Huse, "Scalable probes of measurement-induced criticality," Phys. Rev. Lett. **125**, 070606 (2020).

[29] A. Zabalo, M. J. Gullans, J. H. Wilson, R. Vasseur, A. W. W. Ludwig, S. Gopalakrishnan, David A. Huse, and J. H. Pixley, "Operator scaling dimensions and multifractality at measurement-induced transitions," Phys. Rev. Lett. **128**, 050602 (2022).

[30] Jin Ming Koh, Shi-Ning Sun, Mario Motta, and Austin J. Minnich, "Measurement-induced entanglement phase transition on a superconducting quantum processor with mid-circuit readout," **19**, 1314–1319, number: 9 Publisher: Nature Publishing Group.

[31] Hirsh Kamakari, Jiace Sun, Yaodong Li, Jonathan J. Thio, Tanvi P. Gujarati, Matthew P. A. Fisher, Mario Motta, and Austin J. Minnich, "Experimental demonstration of scalable cross-entropy benchmarking to detect measurement-induced phase transitions on a superconducting quantum processor," Phys. Rev. Lett. **134**, 120401 (2025).

[32] Yuri Minoguchi, Peter Rabl, and Michael Buchhold, "Continuous gaussian measurements of the free boson cft: A model for exactly solvable and detectable measurement-induced dynamics," SciPost Physics **12** (2022), 10.21468/scipostphys.12.1.009.

[33] Kazuki Yokomizo and Yuto Ashida, "Measurement-induced phase transition in free bosons," Physical Review B **111** (2025), 10.1103/y5r3-tv78.

[34] Zejian Li, Anna Delmonte, and Rosario Fazio, "Emergent deterministic entanglement dynamics in monitored infinite-range bosonic systems," Physical Review B **112** (2025), 10.1103/bhst-127b.

[35] Tianci Zhou and Xiao Chen, "Nonunitary entanglement dynamics in continuous-variable systems," Phys. Rev. B **104**, L180301 (2021).

[36] Jordan Huang, Thomas J. DiNapoli, Gavin Rockwood, Ming Yuan, Prathyankara Narasimhan, Eesh Gupta, Mustafa Bal, Francesco Crisa, Sabrina Garattoni, Yao Lu, Liang Jiang, and Srivatsan Chakram, "Fast sideband control of a weakly coupled multimode bosonic memory," (2025), arXiv:2503.10623 [quant-ph].

[37] Ziqian Li, Eesh Gupta, Fang Zhao, Riju Banerjee, Yao Lu, Tanay Roy, Andrew Oriani, Andrei Vrajitoarea, Srivatsan Chakram, and David I. Schuster, "A cascaded random access quantum memory," (2025), arXiv:2503.13953 [quant-ph].

[38] Yvonne Y Gao, Brian J Lester, Yaxing Zhang, Chen Wang, Serge Rosenblum, Luigi Frunzio, Liang Jiang, SM Girvin, and Robert J Schoelkopf, "Programmable interference between two microwave quantum memories," Physical Review X **8**, 021073 (2018).

[39] Scott Aaronson and Alex Arkhipov, "The computational complexity of linear optics," in *Proceedings of the forty-third annual ACM symposium on Theory of computing* (2011) pp. 333–342.

[40] M Kudra, J Biznárová, A Fadavi Roudsari, JJ Burnett, D Niepce, S Gasparinetti, B Wickman, and P Delsing, "High quality three-dimensional aluminum microwave cavities," Applied Physics Letters **117** (2020).

[41] A Romanenko, R Pilipenko, S Zorzetti, D Frolov, M Awida, S Belomestnykh, S Posen, and A Grassellino, "Three-dimensional superconducting resonators at t¡ 20 mk with photon lifetimes up to τ= 2 s," Physical Review Applied **13**, 034032 (2020).

[42] Andrew E Oriani, Fang Zhao, Tanay Roy, Alexander Anferov, Kevin He, Ankur Agrawal, Riju Banerjee, Srivatsan Chakram, and David I Schuster, "Niobium coaxial cavities with internal quality factors exceeding 1.5 billion for circuit quantum electrodynamics," arXiv preprint arXiv:2403.00286 (2024).

[43] Hyejin Kim, Abhishek Kumar, Yiqing Zhou, Yichen Xu, Romain Vasseur, and Eun-Ah Kim, "Learning measurement-induced phase transitions using attention," (2025), arXiv:2508.15895 [quant-ph].

[44] NE Frattini, U Vool, S Shankar, A Narla, KM Sliwa, and MH Devoret, "3-wave mixing josephson dipole element," Applied Physics Letters **110**, 222603 (2017).

[45] Yao Lu, Aniket Maiti, John WO Garmon, Suhas Ganjam, Yaxing Zhang, Jahan Claes, Luigi Frunzio, Steven M Girvin, and Robert J Schoelkopf, "High-fidelity parametric beamsplitting with a parity-protected converter," nature communications **14**, 5767 (2023).

[46] Aniket Maiti, John WO Garmon, Yao Lu, Alessandro Miano, Luigi Frunzio, and Robert J Schoelkopf, "Linear quantum coupler for clean bosonic control," PRX Quantum **6**, 040326 (2025).

[47] Stefan Krastanov, Victor V Albert, Chao Shen, Chang-Ling Zou, Reinier W Heeres, Brian Vlastakis, Robert J Schoelkopf, and Liang Jiang, "Universal control of an oscillator with dispersive coupling to a qubit," Physical Review A **92**, 040303 (2015).

[48] Reinier W. Heeres, Brian Vlastakis, Eric Holland, Stefan Krastanov, Victor V. Albert, Luigi Frunzio, Liang Jiang, and Robert J. Schoelkopf, "Cavity state manipulation using photon-number selective phase gates," **115**, 137002, publisher: American Physical Society.

[49] Alec Eickbusch, Volodymyr Sivak, Andy Z Ding, Salvatore S Elder, Shantanu R Jha, Jayameenakshi Venkatraman, Baptiste Royer, Steven M Girvin, Robert J Schoelkopf, and Michel H Devoret, "Fast universal control of an oscillator with weak dispersive coupling to a qubit," Nature Physics **18**, 1464–1469 (2022).

[50] DI Schuster, Andrew Addison Houck, JA Schreier, A Wallraff, JM Gambetta, A Blais, L Frunzio, J Majer, B Johnson, MH Devoret, *et al.*, "Resolving photon number states in a superconducting circuit," Nature **445**, 515–518 (2007).

[51] Jonas Landgraf, Christa Flhmann, Thomas Fsel, Florian Marquardt, and Robert J. Schoelkopf, "Fast quantum control of cavities using an improved protocol without coherent errors," (2024), arXiv:2310.10498 [quant-ph].

[52] Luyan Sun, Andrei Petrenko, Zaki Leghtas, Brian Vlastakis, Gerhard Kirchmair, KM Sliwa, Aniruth Narla, Michael Hatridge, Shyam Shankar, Jacob Blumoff, *et al.*, "Tracking photon jumps with repeated quantum non-demolition parity measurements," arXiv preprint arXiv:1311.2534 (2013).

[53] Christopher S Wang, Jacob C Curtis, Brian J Lester, Yaxing Zhang, Yvonne Y Gao, Jessica Freeze, Victor S Batista, Patrick H Vaccaro, Isaac L Chuang, Luigi Frunzio, *et al.*, "Efficient multiphoton sampling of molecular vibronic spectra on a superconducting bosonic processor," Physical Review X **10**, 021060 (2020).

[54] See Supplemental Material for additional details.

[55] Fergus Barratt, Utkarsh Agrawal, Andrew C. Potter, Sarang Gopalakrishnan, and Romain Vasseur, "Transitions in the learnability of global charges from local measurements," Physical Review Letters **129** (2022), 10.1103/physrevlett.129.200602.

[56] Hossein Dehghani, Ali Lavasani, Mohammad Hafezi, and Michael J. Gullans, "Neural-network decoders for measurement induced phase transitions," Nature Communications **14** (2023), 10.1038/s41467-023-37902-1.

[57] Ahmed A. Akhtar, Hong-Ye Hu, and Yi-Zhuang You, "Measurement-induced criticality is tomographically optimal," (2023), arXiv:2308.01653 [quant-ph].

[58] Yaodong Li, Yijian Zou, Paolo Glorioso, Ehud Altman, and Matthew P.A. Fisher, "Cross entropy benchmark for measurement-induced phase transitions," Physical Review Letters **130** (2023), 10.1103/physrevlett.130.220404.

[59] Matteo Ippoliti and Vedika Khemani, "Learnability transitions in monitored quantum dynamics via eavesdroppers classical shadows," PRX Quantum **5** (2024), 10.1103/prxquantum.5.020304.

[60] Utkarsh Agrawal, Javier Lopez-Piqueres, Romain Vasseur, Sarang Gopalakrishnan, and Andrew C. Potter, "Observing quantum measurement collapse as a learnability phase transition," Physical Review X **14** (2024), 10.1103/physrevx.14.041012.

[61] Max McGinley, "Postselection-free learning of measurement-induced quantum dynamics," PRX Quantum **5** (2024), 10.1103/prxquantum.5.020347.

[62] Igor Poboiko, Paul Pöpperl, Igor V Gornyi, and Alexander D Mirlin, "Theory of free fermions under random projective measurements," Physical Review X **13**, 041046 (2023).

[63] Kevin S. Chou, Tali Shemma, Heather McCarrick, Tzu-Chiao Chien, James D. Teoh, Patrick Winkel, Amos Anderson, Jonathan Chen, Jacob C. Curtis, Stijn J. de Graaf, John W. O. Garmon, Benjamin Gudlewski, William D. Kalfus, Trevor Keen, Nishaad Khedkar, Chan U. Lei, Gangqiang Liu, Pinlei Lu, Yao Lu, Aniket Maiti, Luke Mastalli-Kelly, Nitish Mehta, Shantanu O. Mundhada, Anirudh Narla, Taewan Noh, Takahiro Tsunoda, Sophia H. Xue, Joseph O. Yuan, Luigi Frunzio, Jos Aumentado, Shruti Puri, Steven M. Girvin, S. Harvey Moseley, and Robert J. Schoelkopf, "A superconducting dual-rail cavity qubit with erasure-detected logical measurements," Nature Physics **20**, 1454–1460 (2024), publisher: Nature Publishing Group.

[64] James D Teoh, Patrick Winkel, Harshvardhan K Babla, Benjamin J Chapman, Jahan Claes, Stijn J de Graaf, John WO Garmon, William D Kalfus, Yao Lu, Aniket Maiti, *et al.*, "Dual-rail encoding with superconducting cavities," Proceedings of the National Academy of Sciences **120**, e2221736120 (2023).

[65] S. Zeytinoglu, M. Pechal, S. Berger, A. A. Abdumalikov, A. Wallraff, and S. Filipp, "Microwave-induced amplitude- and phase-tunable qubit-resonator coupling in circuit quantum electrodynamics," Physical Review A **91** (2015), 10.1103/physreva.91.043846.

[66] Jiasheng Mai, Qiyu Liu, Xiaowei Deng, Yanyan Cai, Zhongchu Ni, Libo Zhang, Ling Hu, Pan Zheng, Song Liu, Yuan Xu, *et al.*, "A biased-erasure cavity qubit with hardware-efficient quantum error detection," arXiv preprint arXiv:2601.21616 (2026).

[67] Serge Rosenblum, P Reinhold, Mazyar Mirrahimi, Liang Jiang, L Frunzio, and RJ Schoelkopf, "Fault-tolerant detection of a quantum error," Science **361**, 266–270 (2018).

[68] Igor Poboiko, Paul Ppperl, Igor V. Gornyi, and Alexander D. Mirlin, "Measurement-induced transitions for interacting fermions," Physical Review B **111** (2025), 10.1103/physrevb.111.024204.

[69] Michele Fava, Lorenzo Piroli, Denis Bernard, and Adam Nahum, "Monitored fermions with conserved $u(1)$ charge," Phys. Rev. Res. **6**, 043246 (2024).

[70] Haoyu Guo, Matthew S. Foster, Chao-Ming Jian, and Andreas W. W. Ludwig, "Field theory of monitored interacting fermion dynamics with charge conservation," Physical Review B **112** (2025), 10.1103/gdxd-pw8v.

[71] Xiangyu Cao, Antoine Tilloy, and Andrea De Luca, "Entanglement in a fermion chain under continuous monitoring," SciPost Physics **7**, 024 (2019).

[72] Michele Fava, Lorenzo Piroli, Tobias Swann, Denis Bernard, and Adam Nahum, "Nonlinear sigma models for monitored dynamics of free fermions," Physical Review X **13** (2023), 10.1103/physrevx.13.041045.

Supplementary Files

This is a list of supplementary files associated with this preprint. Click to download.

- Supplement.zip